

Dark Matter Induced Nucleon Decay Signals in Mesogenesis

Joshua Berger^{1,*} and Gilly Elor^{2,†}

¹Colorado State University, Fort Collins, Colorado 80523, USA

²PRISMA⁺ Cluster of Excellence & Mainz Institute for Theoretical Physics
Johannes Gutenberg University, 55099 Mainz, Germany

We introduce and study the first class of signals that can probe the dark matter in Mesogenesis which will be observable at current and upcoming large volume neutrino experiments. The well-motivated Mesogenesis scenario for generating the observed matter-anti-matter asymmetry necessarily has dark matter charged under baryon number. Interactions of these particles with nuclei can induce nucleon decay with kinematics differing from spontaneous nucleon decay. We calculate the rate for this process and develop a simulation of the signal that includes important distortions due to nuclear effects. We estimate the sensitivity of DUNE, Super-Kamiokande, and Hyper-Kamiokande to this striking signal.

Mesogenesis mechanisms [1–4] utilize the Charge-Parity (CP) violation of Standard Model (SM) meson systems to generate the primordial baryon asymmetry and the dark matter (DM) abundance of the Universe. Excitingly, Mesogenesis is highly testable [5, 6] and experimental searches are underway to probe signals directly linked to the generated baryon asymmetry [6–10] (see overviews in [11–14]). However, a direct probe of the DM in Mesogenesis has remained elusive, until now. In this Letter we study DM induced nucleon decays (IND) in Mesogenesis which can produce a striking signal at current and upcoming neutrino detectors. While the Mesogenesis framework is the primary focus of this letter, the methods developed here can be more broadly applied to search for models containing dark baryons e.g. [15–17].

The novel way in which Mesogenesis satisfies the Sakharov conditions [18], is as follows: mesons produced at late (MeV scale) times, having undergone CP violating processes, decay out of thermal equilibrium into dark baryons. This process generates an equal and opposite baryon asymmetry between the dark and visible sector. For instance, the baryon asymmetry in B^0 -Mesogenesis [1] is generated from the late time production of $B_{s,d}^0$ mesons which undergo CP violating particle-antiparticle oscillations and then quickly decay into a SM baryon and a dark Dirac fermion ψ_B carrying SM baryon number -1 . To evade washing out the generated baryon asymmetry through e.g. $\psi_B \rightarrow p e \bar{\nu}_e$, the ψ_B s must rapidly decay into stable DM states.

Mesogenesis DM consists of two components— a dark Majorana fermion ξ and a dark complex scalar ϕ_B which is charged under SM baryon number. These two stable particles will compose the entirety of the DM. As such the DM halo will consist of a mixture of ξ and ϕ_B particles which can scatter off target nuclei in neutrino detectors to produce mono-energetic pions or kaons and missing energy. This process of IND appears experimentally as nucleon decay but with different kinematics, and as such current limits are essentially not constraining.

The cross section for IND, as it arises in Mesogenesis, will be within reach of neutrino detectors and can be

searched for at the Deep Underground Neutrino Experiment (DUNE) [22], Super-Kamiokande [23], and Hyper-Kamiokande [24]. Furthermore, given the mono-energetic (up to smearing effects) meson, such signals should be distinct over SM backgrounds which primarily consist of mesons produced in atmospheric neutrino processes.

In order to study the details of the IND process, we have developed a Monte Carlo event generation tool within the GENIE [19, 20] software suite used to study accelerator and atmospheric neutrino scattering events [21]. Based on this tool, we are able to study the detailed kinematics of the outgoing mesons produced during DM scattering events and compare these with the dominant atmospheric neutrino scattering background. The event generation includes nuclear effects which smear out the spectrum of mesons from one that is nearly mono-energetic in the non-relativistic DM limit. Furthermore, these events are ready to be used for study in neutrino experiments, where they can be passed through detector-specific simulation software.

In this Letter we first characterize the IND signal. We present the Mesogenesis specific parameter space which can be targeted by experiments. We then detail the simulation. Next, we apply this simulation to estimate the sensitivity of DUNE, Super-Kamiokande, and Hyper-Kamiokande to benchmark models.

Characterizing the IND Signal.— Generating the baryon asymmetry in B -Mesogenesis [1, 3], requires the existence of a TeV scale colored scalar (which may be identified as a squark in a supersymmetric embedding [4]) which mediates the baryon number conserving decay of a B to ψ_B and a SM baryon through the (GeV scale) effective operator:

$$\mathcal{O}_{ab,c} = C_{ab,c} \epsilon_{ijk} \left(u_a^i d_b^j \right) \left(\psi_B d_c^k \right), \quad (1)$$

where all fermions are right handed, though our results easily generalize to left handed operators. $C_{u_a d_b, d_c} \equiv y_{u_a d_b} y_{\psi d_c} / M_Y^2$, where M_Y is the mediator mass. ψ_B decays to the DM through a Yukawa coupling $\mathcal{L}_d \supset y_d \bar{\psi}_B \xi \phi_B + \text{h.c.}$, which is allowed by a stabilizing \mathbb{Z}_2 symmetry under which ψ_B is even and the DM particles odd.

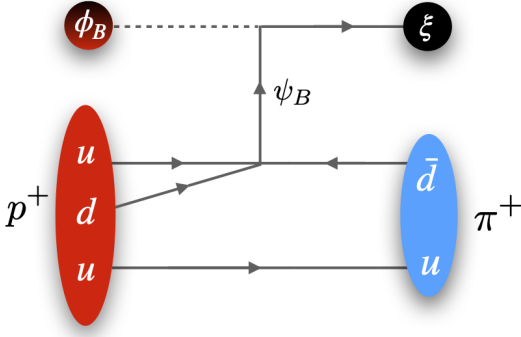


FIG. 1. Induced proton decay to a pion through $\mathcal{O}_{u,dd}$.

Since we remain agnostic about the dark sector, y_d is a free parameter. However a motivated benchmark is $y_d \lesssim \mathcal{O}(0.1)$ which results in the correct DM abundance given an example UV embedding [4].

Eq. 1 generates the IND signal in Mesogenesis: when kinematically allowed, an incoming ξ or ϕ_B scatters off a proton or neutron by exchanging a ψ_B and produces an energetic meson. Fig. 1 depicts an example process — incoming ϕ_B 's induce proton decay to π^+ through $\mathcal{O}_{u,d,d}$. Similarly induced decay to kaons arises through $\mathcal{O}_{u,s,d}$ and $\mathcal{O}_{u,s,d}$. We consider searches at neutrino experiments for the following two processes:

$$\phi_B N \rightarrow \mathcal{M} \xi \quad \text{if } m_{\phi_B} + m_N > m_{\mathcal{M}} + m_{\xi}, \quad (2a)$$

$$\xi N \rightarrow \mathcal{M} \phi_B^* \quad \text{if } m_{\xi} + m_N > m_{\mathcal{M}} + m_{\phi_B}, \quad (2b)$$

where $N = n^0, p^+$ and \mathcal{M} is a SM meson. Recall that ξ is Majorana, allowing any of the DM states to participate in this process when it is kinematically allowed. For decays induced by incoming ϕ_B 's, the kinetic energy of the outgoing meson, to $\mathcal{O}(v_{\text{DM}})$, is given by

$$E_{\phi_B N \rightarrow \xi \mathcal{M}}^{\mathcal{M}, \text{kin}} = \frac{m_{\mathcal{M}}^2 - m_{\xi}^2 + (m_N + m_{\phi_B})^2}{2(m_N + m_{\phi_B})} - m_{\mathcal{M}}. \quad (3)$$

Swap $m_{\xi} \leftrightarrow m_{\phi_B}$ in the above to obtain the meson energy from incoming ξ 's. The expected kinetic energy for each process that arises in Mesogenesis is given in Table I.

If the struck nucleon is at rest, then the outgoing meson is mono-energetic with energy given in Eq (3). However, the nucleons are moving with a momentum of $\mathcal{O}(100 \text{ MeV})$ inside nuclei, smearing out of the meson signal (except for the case of scattering off hydrogen in water Cherenkov detectors). We simulate the IND process, carefully accounting for this smearing. Note that the energies of these decays are shifted compared to spontaneous nucleon decay, with higher energies when ϕ_B scatters and lower energies when ξ scatters. This alters the phenomenology of the Mesogenesis scenario compared with proton decay models such as grand unified theories — the canonical targets of current nucleon decay searches [25–30]. As such, existing limits from nucleon

Initial DM	Final Meson	Mediating Operator	Meson E_{Kin} [GeV]	Approx. $\langle \sigma v \rangle_0$ [cm^3/sec]
ϕ_B	π^+/π^0	$\mathcal{O}_{u,d,d}$	0.6 - 1.2	$10^{-21.4} - 10^{-21.0}$
ξ	π^+/π^0	$\mathcal{O}_{u,d,d}$	0.02 - 0.6	$10^{-22.5} - 10^{-21.9}$
ϕ_B	K^+/K^0	$\mathcal{O}_{u,s,d}, \mathcal{O}_{u,d,s}$	0.3 - 0.9	$10^{-19.7} - 10^{-19.3}$
ξ	K^+/K^0	$\mathcal{O}_{u,s,d}, \mathcal{O}_{u,d,s}$	0.04 - 0.3	$10^{-20.6} - 10^{-19.8}$

TABLE I. The induced nucleon decays allowed by kinematics (2) and Mesogenesis considerations Eq. 5. We show the corresponding flavorful variation of the operator Eq. 1 that generates the decay, the expected range of un-smearred kinetic energy of the outgoing meson computed from Eq. (3), and the stripped cross section defined in Eq. (6).

decay searches, with a few exceptions, do not constrain the Mesogenesis signal. Similar considerations were discussed in the context of Hylogenesis [31].

The cross section for IND is obtained from the matrix element:

$$\begin{aligned} \mathcal{A}_{\phi_B N \rightarrow \xi \mathcal{M}} &= \bar{u}_{\xi}(\vec{p}_{\xi}) \frac{y_d C_{ab,c}}{p_{\psi_B}^2 - m_{\psi_B}^2} \left(\not{p}_{\psi_B} + m_{\psi_B} \right) \quad (4) \\ &\times P_R \left[W_0^{RR} - i \frac{\not{p}_{\psi_B}}{m_N} W_1^{RR} \right] u_N(\vec{p}_N), \end{aligned}$$

with $\bar{u}_{\xi} \rightarrow \bar{v}_{\xi}$ for $\xi N \rightarrow \mathcal{M} \phi_B^*$. Here, $p_{\psi_B} = p_{\xi} - p_{\phi_B}$ and P_R is the right handed fermion projector. The Wilson Coefficients are constrained by a combination of LHC searches for the mediator and flavor observables: $C_{u,d,d}^{\text{max}} = 0.07 \text{ TeV}^{-2}$ and $C_{u,s,d}^{\text{max}}, C_{u,d,s}^{\text{max}} = 0.64 \text{ TeV}^{-2}$ [6, 15]. Since INDs can lead to $\mathcal{O}(\text{GeV})$ momentum transfer, we use high q^2 extrapolated lattice results from [32] for the form factors $W_{0,1}^{RR}$ [33]. Including the momentum dependence of $W_{1,2}$ negligibly affects the signal. The $\mathcal{O}_{u,s,d}$ and $\mathcal{O}_{u,d,s}$ require different form factors but lead to similar signals.

Mesogenesis Parameter Space.— In addition to the kinematic constraints on IND Eq. (2), the allowed parameter space is constrained by Mesogenesis-specific considerations i.e. generating the observed baryon asymmetry and DM abundance:

$$m_{\phi_B} + m_{\xi} < m_{\psi_B} < m_B - m_p \simeq 4.34 \text{ GeV}, \quad (5a)$$

$$|m_{\phi_B} - m_{\xi}| < m_p + m_e \simeq 938.8 \text{ MeV}, \quad (5b)$$

$$m_{\psi_B}, m_{\phi_B} > m_p - m_e. \quad (5c)$$

$$m_{\phi_B} > m_{\xi}. \quad (5d)$$

The regions in $\{m_{\xi}, m_{\phi_B}\}$ space excluded by these constraints are shaded in Fig. 2, while the white region is allowed. Eq. (5a) ensured that ψ_B is light so that the baryon asymmetry can be generated through the decay $B \rightarrow \mathcal{B}_{\text{SM}} + \psi_B$, while also being heavy enough to decay into the DM ξ and ϕ_B . Decreasing the value of m_{ψ_B} corresponds to increasing the excluded green region. For $m_{\psi_B} \simeq 1.1 \text{ GeV}$, there is no longer viable parameter space. Eq. (5b) is enforced to prevent ξ and ϕ_B from coalescing into SM baryons, which would washout the

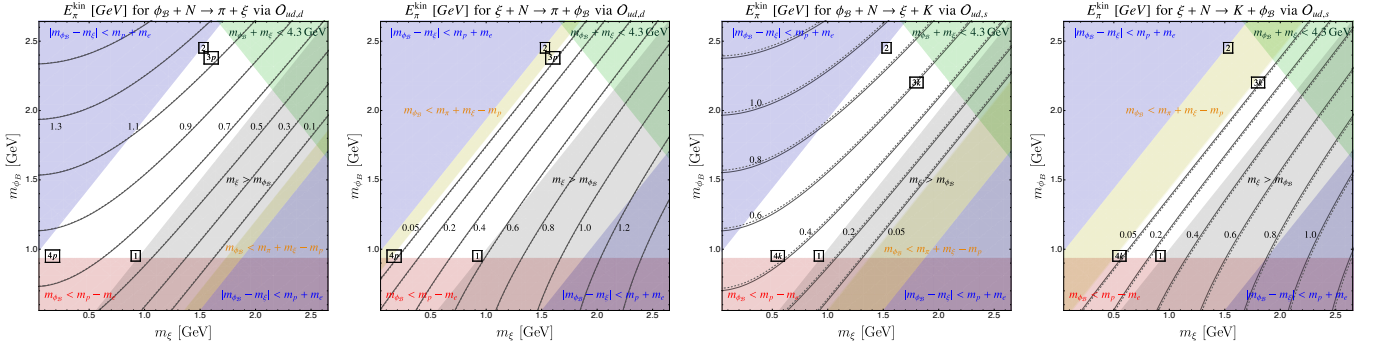


FIG. 2. Parameter space and kinetic energy contours for the eight different DM IND processes arising in Mesogenesis. Colored regions are ruled out by kinematics Eq. (2) or mechanism considerations Eq. (5). Solid lines correspond to kinetic energy for scattering off protons $N = p$, and the dashed off nucleons $N = n$. In each panel, we indicate the location of the representative benchmark points: 1, 2, 3p, 4p for pions and 1, 2, 3k, 4k for kaons as summarized in Table II.

baryon asymmetry. Proton decay through Eq. (1) to dark baryons is kinematically forbidden through Eq. (5c). A complete list of DM IND processes consistent with Eq. (2) and Eq. (5) is shown in Table I.

There must exist dark sector interactions which deplete the DM and ensure the correct abundance [1]. Since $n_{\phi_B} - \bar{n}_{\phi_B}$ is related to the baryon asymmetry, ϕ_B must always constitute some, but not all, of the DM: if $m_{\phi_B} < m_\xi$, dark interactions could annihilate the entire ξ population into ψ_B . The measured ratio of DM to baryon densities [34] implies that $m_{\phi_B} \simeq 5m_p$, violating Eq. (5a). This motivates multi-component DM where we enforce Eq. 5d so that the symmetric component of ϕ_B annihilate into ξ s. Since the measured SM baryon asymmetry is always balanced by an asymmetry in ϕ_B s, the observed DM to baryon ratio $\rho_{\text{DM}} \sim 5\rho_B$ fixes the expected density of ξ and ϕ_B particles in the halo: $\rho_\xi/\rho_{\phi_B} = 5m_p/m_{\phi_B} - 1$, and $\rho_{\text{total}} = \rho_\phi + \rho_\xi = 0.4 \text{ GeV/cm}^3$. Given Eq. (5c), there will always be a substantial asymmetric component of DM, and so both INDs in Eq. (2) will be present if kinematically allowed.

The scattering cross sections for the INDs are computed from Eq. (4). They scale roughly as $\langle\sigma v\rangle \propto m_{\psi_B}^{-2}$, but the range of variation $m_{\psi_B} \sim 1\text{--}4.3 \text{ GeV}$, leads to a small effect. We parametrize the cross section as:

$$\langle\sigma v\rangle_{\text{DM}}^{\mathcal{M}} \equiv \frac{(y_d \times C_{ud_i, d_j})^2}{m_{\psi_B}^2 [\text{GeV}^{-4}]} \langle\sigma v\rangle_{\text{DM}}^{\mathcal{M}, 0} \quad (6)$$

where $\mathcal{M} = \pi^0, \pi^+, K^+, K^0$ and $\text{DM} = \phi_B, \xi$. Values of the coupling stripped cross section $\langle\sigma v\rangle_{\text{DM}}^{\mathcal{M}, 0}$ over the allowed parameter space of Fig. 2) are shown in Table I. For e.g. $y_d = 0.1$ and $C_{ud_i, d_j}^{\text{max}}$, the expected cross section can be as large as $10^{-38} - 10^{-36} \text{ cm}^3/\text{sec}$ in the allowed parameter space for all channels. Meanwhile, the estimated sensitivity at DUNE and Super-Kamiokande is roughly $10^{-42} - 10^{-40} \text{ cm}^2/\text{sec}$.

Benchmark	m_{ϕ_B} [GeV]	m_ξ [GeV]
1	0.95	0.92
2	2.45	1.53
3p	2.38	1.6
3k	2.2	1.8
4p	0.95	0.17
4k	0.95	0.55

TABLE II. Benchmarks highlighting the possible signal topologies. Benchmark 1 corresponds to $E_{p\phi_B \rightarrow \mathcal{M}\xi}^{\text{kin}, \text{min}} \sim E_{p\phi_B \rightarrow \mathcal{M}\xi}^{\text{kin}, \text{max}}$ for both π s and kaons. Benchmark 2 corresponds to $E_{p\phi_B \rightarrow \mathcal{M}\xi}^{\text{kin}, \text{max}}$. Benchmarks 3p and 3k correspond to the maximal $E_{p\phi_B \rightarrow \mathcal{M}\xi}^{\text{kin}}$ such that the incoming ξ process is still allowed for production of π s and kaons respectively. Benchmarks 4p and 4k highlight a region of $\{m_\xi, m_{\phi_B}\}$ which would still lead to a signal for small m_{ψ_B} (see also labels in Fig 2).

Signal Monte Carlo and Benchmarks.— Non-relativistic DM striking a nucleon at rest and inducing decay would lead to a mono-energetic signal with kinetic energy given by Eq. (3) and shown in Fig. 2. We pick benchmark points to highlight the possible signal topologies; these are defined in Table II and labeled in Fig. 2. In the context of large nuclei, nuclear effects including nuclear motion of the nucleons and final state interactions of hadronic particles escaping the nuclear remnant smear the outgoing meson energy, can liberate additional hadrons, and can change the isospin characteristics of the meson. In order to account for these effects, as well as allow for future simulation of the detailed detector response at neutrino experiments, we have developed a Monte Carlo event generation tool for the IND process.

Signal events are generated using a modified version of GENIE v3.0.2 [19, 20]. We employ the default tune (G18_02a) throughout, though we considered other nuclear models. We found differences in the signal distributions of order 10% between hA and hN models of the intranuclear cascade. The current nucleon decay mod-

ule in **GENIE** was modified to allow for IND kinematics. The meson final states currently implemented are π^0 , π^\pm , $K_{S/L}^0$, K^\pm , and D^0 . This module propagates the outgoing mesons through the nuclear remnant to the edge of the nucleus. The kinematics of the IND process is fixed given masses for the two DM particles. The cross section is determined by Eq. (6). For non-relativistic DM, there is a small difference in the rate for interaction with a high speed nucleon compared with a nucleon at rest. We neglect this small difference of $\sim 10\%$.

Signals at Neutrino Experiments. — The current best limits on spontaneous nucleon decays to pions are from a Super-Kamiokande [27], which applied a pion momentum cut of 1 GeV and is thus applicable to parts of Mesogenesis parameter space — here the experimental limit can be compared to an effective lifetime $(\tau_N^{\text{ind}})^{-1} = n_{\text{DM}} \langle \sigma v \rangle_{\text{DM}}$ [31, 35, 36]. This yields an approximate, conservative, limit of $y_d \times C_{ud,d} / C_{ud,d}^{\text{max}} \gtrsim 0.03 - 0.1$ for $70 \text{ MeV} \lesssim E_{\pi^\pm}^{\text{kin}} \lesssim 870 \text{ MeV}$ and $E_{\pi^0}^{\text{kin}} \lesssim 870 \text{ MeV}$. Existing searches in kaon channels [29, 30] placed narrow ranges of momentum cuts. Consequentially, the majority of parameter space of interest is unconstrained by existing searches. Super-Kamiokande is expected to have sensitivity to IND signals given *dedicated* studies. Hyper-Kamiokande will improve on this with its larger exposure. Since DUNE is based on liquid argon time-projection chamber (LArTPC) technology, it could have particular sensitivity to certain models.

We assume kinetic energy thresholds as indicated in Table III, based on the studies where available [37] and otherwise based on Cherenkov thresholds or detecting tracks/showers in LArTPCs. Determining reconstruction efficiencies requires a dedicated study by the respective experimental collaborations. In Super-Kamiokande’s search for proton decay in the $\pi^+\nu$ channel, no muon/pion separation was attempted [27]. On the other hand, the LArTPC experiment MicroBooNE has demonstrated muon/pion separation at the 80% level [38], consistent with other particle identification efficiencies. We therefore do not assume muon/pion separation for the Water Cherenkov experiments, while we assume perfect muon/pion separation for DUNE. Searches for similar signals of kaons in spontaneous nucleon decay at Super-Kamiokande indicate reconstruction efficiencies around or below 10% [29, 30]. The full 3D imaging of LArTPC detectors like DUNE may increase performance in reconstructing complex topologies arising from kaon decays, e.g. kaons above 40 MeV kinetic energy may be efficiently be reconstructed as tracks before decay [39].

Sensitivity Estimate. — The dominant background for the channels we consider is expected to be inelastic scattering of atmospheric neutrinos off nuclei, leading to additional mesons. By looking for off beam timing events, beam-related backgrounds can be evaded. To study the atmospheric neutrino background, we generate atmospheric neutrino events using **GENIE** v3.0.2, along

Particle	LArTPC Thresh. [MeV]	Cherenkov Thresh. [MeV]
e^\pm	30	3.5
γ	30	3.5
μ^\pm	35	55
π^\pm	35	72
p	80	481

TABLE III. Kinetic energy thresholds for particles assumed in LArTPC (DUNE) and Water Cherenkov (Super- and Hyper-Kamiokande) detectors.

with the Bartol atmospheric neutrino flux model [40] at Soudan for DUNE and Kamioka.

From samples of DM signals and atmospheric neutrino events, we look for events containing the relevant final state meson for the channel considered. Not all events with such a meson should be considered. Signal events contain a single meson and no other activity other than possible emissions from the nuclear remnant or byproducts of final state interactions. Thus, it is highly beneficial to veto any activity beyond the expected meson. To do so, we first apply the thresholds in Table III to all final state particles. Of the remaining particles that can be detected, we veto on events that have anything other than a meson of the expected type. For the pion channels, order 1% of atmospheric neutrino scattering events lead to an event matching these criteria. This leaves a search that is not entirely background free. For the kaon channels on the other hand, single kaon events are only possible with additional flavor-violating weak interactions. Searches in these channels may thus be background free if kaon reconstruction is sufficiently good. To get a sense of the events after these vetoes we plot kinetic energy distributions of the remaining signal and background events; a few illustrative distributions are shown in Fig. 3.

We now estimate the sensitivity to $y_d \times C_{ud_i,d_j} / C_{ud_i,d_j}^{\text{max}}$. For pion channels, we apply the selection described above. To eliminate a majority of the background events, we also require that the selected pion has a kinetic energy within 100 MeV of its unsmeared value Eq. (3). For the kaon channels, no further selection is required as we have found that this channel is nearly background free, and we determine the coupling that would lead to 5 signal events over the assumed exposure of the experiment. In cases where there is background, we estimate the 2σ sensitivity to the signal. The sensitivity results are summarized in Table IV for the benchmarks listed in Table II.

Discovering an IND signal would be a direct probe of the DM in Mesogenesis. In addition to providing experimentalists with the tools needed to search for DM IND signals at neutrino experiments, this letter paves the way to a signal driven model building effort of the dark sector.

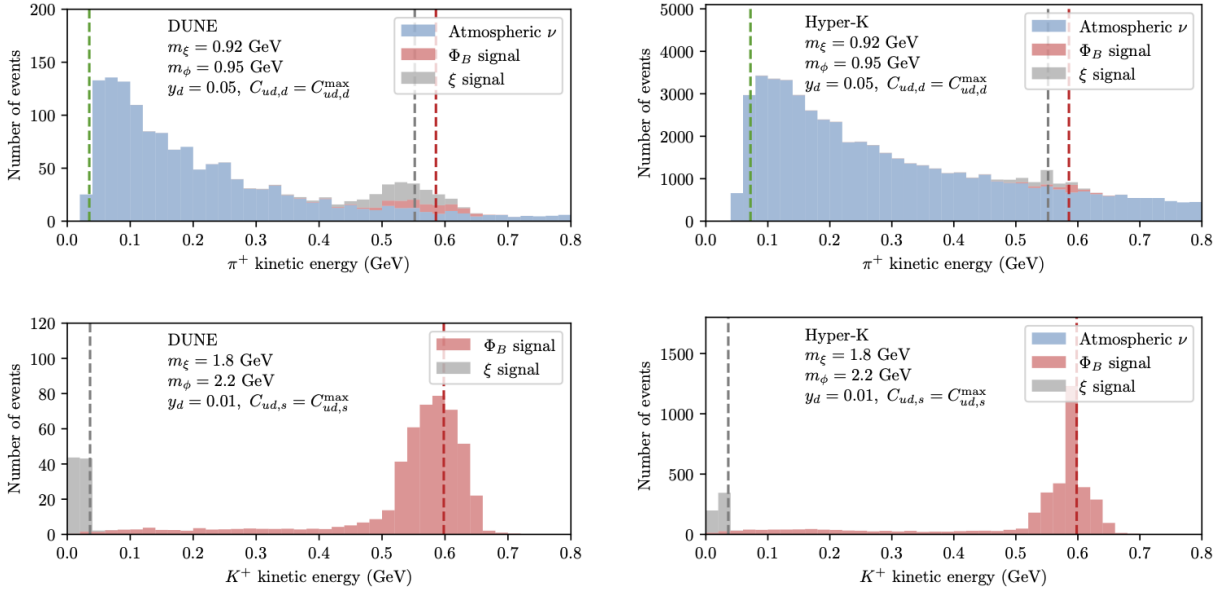


FIG. 3. Kinetic energy distributions for sample benchmark models at DUNE and Hyper-Kamiokande. Super-Kamiokande, is simply a rescaling of the rate at Hyper-Kamiokande by a factor of 16. Dashed lines indicate the un-smearred energy Eq. 3. Green lines indicate, where relevant, the assumed threshold for the detector to see the meson. The top row correspond to Benchmark 1, while the bottom corresponds to Benchmark 3k. The Hyper-Kamiokande signal has a noticeable mono-energetic spike corresponding to scattering of hydrogen, while the smeared distribution corresponds to scatterings off oxygen.

Benchmark and Meson	Background	$y_d(C_{ud_i,d_j}/C_{ud_i,d_j}^{\max})$	Background	$y_d(C_{ud_i,d_j}/C_{ud_i,d_j}^{\max})$	Background	$y_d(C_{ud_i,d_j}/C_{ud_i,d_j}^{\max})$
	DUNE	DUNE sensitivity	Super-K	Super-K sensitivity	Hyper-K	Hyper-K sensitivity
1 π^+	118	0.019	1759	0.030	9452	0.020
2 π^+	14	0.007	432	0.014	2323	0.0090
3p π^+	584	0.021	2570	0.023	13835	0.015
4p π^+	600	0.040	2907	0.045	15653	0.029
1 π^0	140	0.025	125	0.026	672	0.017
2 π^0	26	0.011	17	0.011	94	0.0069
3p π^0	915	0.080	590	0.080	3135	0.052
4p π^0	923	0.053	608	0.050	3231	0.033
1 K^+	0	0.0016	0	0.0014	0	0.00061
2 K^+	0	0.00038	0	0.00032	0	0.00014
3k K^+	0	0.00063	0	0.00054	0	0.00023
4k K^+	0	0.0010	0	0.00087	0	0.00038
1 K_S^0	0	0.00047	0	0.00056	0	0.00024
2 K_S^0	0	0.00034	0	0.00041	0	0.00018
3k K_S^0	0	0.00037	0	0.00044	0	0.00019
4k K_S^0	0	0.00049	0	0.00058	0	0.00025

TABLE IV. Estimated coupling sensitivity at DUNE with 400 kton-years of exposure, at Super-Kamiokande with 350.8 kton-years of exposure, and at Hyper-Kamiokande with 1,900 kton-years of exposure. We apply the solar minimum flux model for all experiments. The solar maximum model gives slightly different sensitivity estimates.

We thank Yun-Tse Tsai for comments on the draft and Yue Zhao for helpful discussions. The work of J.B. is supported by the National Science Foundation under Grant No. 2112789. G.E. is supported by the Cluster of Excellence *Precision Physics, Fundamental Interactions and Structure of Matter* (PRISMA⁺ – EXC 2118/1) within the German Excellence Strategy (project ID 39083149).

J.B. thanks the Mainz Institute for Theoretical Physics (MITP) of the Cluster of Excellence PRISMA⁺ (project ID 39083149) for their hospitality.

-
- * Joshua.Berger@colostate.edu
† gelor@uni-mainz.de
- [1] G. Elor, M. Escudero, and A. Nelson, *Phys. Rev. D* **99**, 035031 (2019), arXiv:1810.00880 [hep-ph].
- [2] G. Elor and R. McGehee, *Phys. Rev. D* **103**, 035005 (2021), arXiv:2011.06115 [hep-ph].
- [3] F. Elahi, G. Elor, and R. McGehee, *Phys. Rev. D* **105**, 055024 (2022), arXiv:2109.09751 [hep-ph].
- [4] G. Alonso-Álvarez, G. Elor, A. E. Nelson, and H. Xiao, *JHEP* **03**, 046 (2020), arXiv:1907.10612 [hep-ph].
- [5] G. Elor and A. W. M. Guerrero, (2022), arXiv:2211.10553 [hep-ph].
- [6] G. Alonso-Álvarez, G. Elor, and M. Escudero, *Phys. Rev. D* **104**, 035028 (2021), arXiv:2101.02706 [hep-ph].
- [7] C. Hadjivasiliou *et al.* (Belle), *Phys. Rev. D* **105**, L051101 (2022), arXiv:2110.14086 [hep-ex].
- [8] A. B. Rodriguez, V. Chobanova, X. Cid Vidal, S. L. Solino, D. M. Santos, T. Mombacher, C. Prouve, E. X. R. Fernandez, and C. Vazquez Sierra, *Eur. Phys. J. C* **81**, 964 (2021), arXiv:2106.12870 [hep-ph].
- [9] M. Borsato *et al.*, *Rept. Prog. Phys.* **85**, 024201 (2022), arXiv:2105.12668 [hep-ph].
- [10] X. Shi (BESIII), *PoS EPS-HEP2021*, 663 (2022).
- [11] G. Elor *et al.*, in *2022 Snowmass Summer Study* (2022) arXiv:2203.05010 [hep-ph].
- [12] P. Asadi *et al.*, (2022), arXiv:2203.06680 [hep-ph].
- [13] J. L. Barrow *et al.*, (2022), arXiv:2203.07059 [hep-ph].
- [14] E. Goudzovski *et al.*, (2022), arXiv:2201.07805 [hep-ph].
- [15] G. Alonso-Álvarez, G. Elor, M. Escudero, B. Fornal, B. Grinstein, and J. Martin Camalich, *Phys. Rev. D* **105**, 115005 (2022), arXiv:2111.12712 [hep-ph].
- [16] B. Fornal and B. Grinstein, *Mod. Phys. Lett. A* **35**, 2030019 (2020), arXiv:2007.13931 [hep-ph].
- [17] B. Grinstein, C. Kouvaris, and N. G. Nielsen, *Phys. Rev. Lett.* **123**, 091601 (2019), arXiv:1811.06546 [hep-ph].
- [18] A. D. Sakharov, *Pisma Zh. Eksp. Teor. Fiz.* **5**, 32 (1967), [*Usp. Fiz. Nauk*161,61(1991)].
- [19] C. Andreopoulos *et al.*, *Nucl. Instrum. Meth. A* **614**, 87 (2010), arXiv:0905.2517 [hep-ph].
- [20] C. Andreopoulos, C. Barry, S. Dytman, H. Gallagher, T. Golan, R. Hatcher, G. Perdue, and J. Yarba, (2015), arXiv:1510.05494 [hep-ph].
- [21] All data generated using this code is available upon request. The code itself can be downloaded from <https://github.com/jberger7/Generator-IND>.
- [22] M. N. Guinot (DUNE), *PoS NuFact2021*, 231 (2022).
- [23] C. W. Walter, , 19 (2008), arXiv:0802.1041 [hep-ex].
- [24] M. Yokoyama (Hyper-Kamiokande Proto), in *Prospects in Neutrino Physics* (2017) arXiv:1705.00306 [hep-ex].
- [25] C. McGrew *et al.*, *Phys. Rev. D* **59**, 052004 (1999).
- [26] D. Wall *et al.* (Soudan 2), *Phys. Rev. D* **62**, 092003 (2000), arXiv:hep-ex/0001015.
- [27] K. Abe *et al.* (Super-Kamiokande), *Phys. Rev. Lett.* **113**, 121802 (2014), arXiv:1305.4391 [hep-ex].
- [28] K. Abe *et al.* (Super-Kamiokande), *Phys. Rev. D* **95**, 012004 (2017), arXiv:1610.03597 [hep-ex].
- [29] K. Kobayashi *et al.* (Super-Kamiokande), *Phys. Rev. D* **72**, 052007 (2005), arXiv:hep-ex/0502026.
- [30] K. Abe *et al.* (Super-Kamiokande), *Phys. Rev. D* **90**, 072005 (2014), arXiv:1408.1195 [hep-ex].
- [31] H. Davoudiasl, D. E. Morrissey, K. Sigurdson, and S. Tulin, *Phys. Rev. D* **84**, 096008 (2011), arXiv:1106.4320 [hep-ph].
- [32] Y. Aoki, T. Izubuchi, E. Shintani, and A. Soni, *Phys. Rev. D* **96**, 014506 (2017), arXiv:1705.01338 [hep-lat].
- [33] The corresponding values of $W_0(W_1)$ for π^+ are $0.038\sqrt{2}$ ($-0.05\sqrt{2}$), for π^0 are 0.038 (-0.05), and, through $\mathcal{O}_{ud,s}$, for K^+ are 0.0648 (-0.046) and for K^0 are -0.0648 (0.046).
- [34] N. Aghanim *et al.* (Planck), *Astron. Astrophys.* **641**, A6 (2020), [Erratum: *Astron. Astrophys.* 652, C4 (2021)], arXiv:1807.06209 [astro-ph.CO].
- [35] H. Davoudiasl, D. E. Morrissey, K. Sigurdson, and S. Tulin, *Phys. Rev. Lett.* **105**, 211304 (2010), arXiv:1008.2399 [hep-ph].
- [36] J. Huang and Y. Zhao, *JHEP* **02**, 077 (2014), arXiv:1312.0011 [hep-ph].
- [37] K. Abe *et al.* (Super-Kamiokande), *Phys. Rev. D* **94**, 052010 (2016), arXiv:1606.07538 [hep-ex].
- [38] J. N. Esquivel, *μ/π Separation using Convolutional Neural Networks for the MicroBooNE Charged Current Inclusive Cross Section Measurement*, Ph.D. thesis, Syracuse U., Syracuse U. (2018).
- [39] B. Abi *et al.* (DUNE), *Eur. Phys. J. C* **81**, 322 (2021), arXiv:2008.12769 [hep-ex].
- [40] G. D. Barr, T. K. Gaisser, P. Lipari, S. Robbins, and T. Stanev, *Phys. Rev. D* **70**, 023006 (2004), arXiv:astro-ph/0403630.